Near-Infrared Silicon Photonic Crystals with High-Order Photonic Bandgaps for High-Sensitivity Chemical Analysis of Water-Ethanol Mixtures

Journal:	*ACS Sensors*
Manuscript ID	se-2018-00933j.R1
Manuscript Type:	Letter
Date Submitted by the Author:	26-Oct-2018
Complete List of Authors:	Surdo, Salvatore; University of Pisa (IED/UNIPI), Information Engineering Department Carpignano, Francesca; ST Microelectronics Merlo, Sabina; Universita degli Studi di Pavia, Ingegneria Industriale e dell'Informazione Barillaro, Giuseppe; University of Pisa (IED/UNIPI), Information Engineering Department

Near-Infrared Silicon Photonic Crystals with High-Order Photonic Bandgaps for High-Sensitivity Chemical Analysis of Water-Ethanol Mixtures

Salvatore Surdo[1,2], Francesca Carpignano[3,4], Sabina Merlo[3] and Giuseppe Barillaro[1]*

[1]Dipartimento di Ingegneria dell'Informazione, Università di Pisa, via G. Caruso 16, 56122 Pisa, Italy.

[2]Nanophysics, Istituto Italiano di Tecnologia, via Morego 30, 16123, Genova, Italy.

[3]Dipartimento di Ingegneria Industriale e dell'Informazione, Università di Pavia, Pavia 27100, Italy.

[4]MEMS Technology Development, AMG Group, STMicroelectronics, Via C. Olivetti, 2, Agrate Brianza 20041, Italy.

*Corresponding author: giuseppe.barillaro@iet.unipi.it

Abstract

Aqueous solutions of alcohols are used in several applications, from pharmaceutics and biology, to chemical, biofuel, and food industries. Nonetheless, development of a simple, inexpensive, and portable sensing device for the quantification of water in water-ethanol mixtures remains a significant challenge. Photonic crystals (PhCs) operating at very high-order bandgaps (PBGs) offer remarkable opportunities for the realization of chemical sensors with high sensitivity and low detection limit. However, high-order PhC structures have been mostly confined to mere theoretical speculations so far, their effective realization requiring microfabrication tools enabling the control of periodic refractive index modulations at the sub-micrometric scale with extremely high both accuracy and precision.

Here, we report both experimental and theoretical results on high-sensitivity chemical analysis using vertical, silicon/air 1D-PhCs with spatial period of 10 and 20 μm (namely, over 10 times the operational wavelength) featuring ultra-high-order PBGs in the near-infrared region (namely, up to 50th at 1.1 μm). Fabrication of high-order 1D-PhCs is carried out by electrochemical micromachining (ECM) of silicon,

which allows both surface roughness and deviation from verticality of etched structures to be controlled below 5 nm and 0.1%, respectively. Optical characterization of ECM-fabricated 1D-PhCs is carried out by acquiring reflectivity spectra over the wavelength range 1-1.7 μm, which allows the presence of ultra-high-order PBGs with minor optical losses (i.e. <1 dB in reflectivity) separated by deep reflectivity notches with high Q-factors (i.e. >6000) to be appreciated, in good agreement with theoretical results. Eventually, we investigated the use of high-order 1D-PhCs for the refractometric quantitative detection of trace of water in water-ethanol mixtures, demonstrating that a high sensitivity (namely, either 1000 nm/RIU or ~0.4 nm/% of water), good detection limit (namely, 5×10^{-3} RIU or ~10% water), and excellent resolution (namely, either 6×10^{-4} RIU or 1.6% of water) is reliably achieved on a detection volume of about 168 fL.

Keywords: photonic crystals, high aspect ratio, electrochemistry, micromachining, refractometry, chemical analysis, water-ethanol mixtures.

Aqueous solutions of alcohols are used in several applications, from pharmaceutics to biological sciences, from chemical and biofuel industries to food and beverage farms.[1,2] Therefore, determining the water content in aqueous alcohol solutions with high sensitivity is of chief importance for chemicals, pharmaceuticals and food preparation. The standard laboratory method for determining the amount of water in a water-ethanol mixture is Karl-Fischer titration.[3] Although this method represents the gold standard, it requires trained personnel, it is time-consuming, and reagents are toxic. Besides, both chromatography[4] and infrared spectroscopy[5] are routinely used as they do not involve toxic reagents, though they do not allow for in-line and real-time monitoring of hydro alcoholic solutions.

In order to overcome the limitations of the methods described above, recent research has focused on developing highly sensitive approaches for the in-situ and in real-time analysis of water content in organic solvents. Among the different approaches, electrical (e.g. capacitors,[6,7] resonators[8,9]) and optical

(e.g. fluorescent/colorimetric,[2,10,11] photonic/plasmonic[12,13]) methods have been successfully reported. Among these, optical methods either exploit specific chemical reactions with water to enhances fluorescence and color changes or do monitor refractive index changes[2,10,11] of the water-alcohol mixture using highly sensitive optical transducers,[12,13] with advantage of higher sensitivity, lower detection limit, larger range, and improved portability with respect to electrical approaches. Nonetheless, development of a simple, inexpensive, and portable sensing device for the quantification of water in water-ethanol mixtures remains a significant challenge.

To the best of our knowledge, little research has been done on utilizing the fascinating phenomenon of forbidden propagation of light in photonic crystals (PhCs) for the quantification of water in water-ethanol mixtures.[14–18]

Photonic crystals, either natural or artificial materials with a periodic modulation of the refractive index at the micro and nanoscale, offer remarkable opportunities for optical sensing of both chemicals and biological matters.[19–23] In fact, any physicochemical process occurring in the presence of the chemical/biological matter and affecting the refractive index of the materials assembling the PhC structure causes a change of the PhC optical spectrum that can be effectively quantified.

This capability has been successfully used to implement optical sensors with high sensitivity and low detection limit, [20,24–29] mostly accomplished using PhCs exploiting either evanescent or guided modes, such as PhC slabs and waveguides, to probe the chemical/biological sample delivered by flow-over microfluidics. Nonetheless, the small penetration depth of evanescent waves and the slow diffusion kinetics of molecules weakens interaction of light and chemical/biological matter in these PhC structures, limiting, in turn, the ultimate sensitivity of the optical sensors exploiting such structures as refractive index transducers.

Higher sensitivity has been achieved when the chemical/biological sample is flown through the PhC structure, thanks to an enhanced light-matter interaction.[14,30–32] This strategy has been shown to be highly effective when PhC resonant cavities are used as refractive index transducers,[33–35] for which the

presence of a defect breaking the PhC periodicity gives rise to a sharp (i.e. with high quality factor, Q) resonance peak that enhances sensitivity and lowers, in turn, detection limit.[36] On the other hand, because of the high interaction strength between optical field and cavity defect, any fabrication errors affecting either position or size of the cavity defect have a significant impact on the optical features of resonant cavity and, in turn, on the performance of the optical sensors based on these structures.[37]

Recently, high-sensitivity in chemical/biological analysis has been demonstrated using flow-through vertical PhC structures supporting high-order photonic bandgaps (PBGs).[15,18,38]

Noteworthy, high-order PhCs feature a refractive index modulation whose spatial period is longer than the operation wavelength, therefore relaxing the fabrication process of these structures with respect to PhCs exploiting either the fundamental or low-order PBGs. Nonetheless, both accuracy and reproducibility of morphological features (e.g. spatial period, material thickness, surface roughness) still play a crucial role toward the experimental achievement of PhCs with high-order PBGs. In fact, the occurrence of structural disorders, such as change of the spatial period or presence of rough interfaces over the PhC structure, produces incoherent interference and light scattering throughout the periodic structure, respectively, which easily degrades high-order optical features of the PhC structure, such as PBGs, extinction-ratio (i.e. Q factor) between high and low-reflectivity bands, both in reflection and transmission.

Among other state-of-the-art micro and nanofabrication technologies, silicon electrochemical micromachining (ECM) has been recently shown to enable the fabrication of vertical silicon/air 1D-PhC with high-order bandgaps (i.e. up to 20th order) in the near-infrared region, both for telecom application and chemical/biological analysis.[15,18,39] Indeed, this technology allows the anodic dissolution of silicon in acidic (HF-based) aqueous electrolytes to be controlled with sub-micrometric accuracy and nanometric surface roughness, also providing high flexibility in terms of geometrical features, namely trenches, pores, pillars, spirals.[40–43]

Vertical silicon/air 1D-PhCs with high-order photonic bandgaps fabricated by ECM technology have been successfully used for refractometry. These structures inherently feature independent optical (perpendicular to the Si walls) and fluidic (parallel to the air-gaps) paths, which enable the incorporation of high-order PhC transducers into advanced optofluidic platforms, integrating, for instance, grooves for accurate optical-fiber positioning in front of PhCs and microfluidic channels for the convective transport of target fluids and analytes within the PhCs. Furthermore, the unique combination of a high refractive index contrast (between crystalline silicon and liquid to be analyzed) with high-order photonic bandgaps in high-order PhCs results in a reflection/transmission spectrum with sharp high-Q (>1000) notches/peaks, which enable tiny changes in their spectral position due to light interaction with chemical/biological matter to be effectively monitored.

Here, we report both experimental and theoretical results on silicon 1D-PhCs with ultra-high-order PBGs (from 34^{th} at 1.6 μm up to 50^{th} at 1.1 μm) in the near-infrared region, with application to quantitative water detection in water-ethanol mixtures. To the best of our knowledge, this is the highest order of PBGs that has been experimentally reported so far, either with silicon or other materials, thus narrowing the gap between theoretical and experimental findings in the PhC area. In particular, vertical 1D-PhCs with spatial period of 10 and 20 μm, surface roughness below 5 nm, and deviation from verticality of 0.1% were successfully etched in silicon by ECM technology. A thorough optical characterization of 1D-PhCs clearly highlighted the presence of ultra-high-order PBGs with minor optical losses (i.e. <1 dB in reflectivity), separated by deep reflectivity notches with high Q-factors (i.e. >6000), in very good agreement with theoretical calculations. The use of ultra-high-order 1D-PhCs for quantitative water detection in water-ethanol mixtures by refractometry, pointed out that high-order 1D-PhCs allow high sensitivity (i.e., 1000 nm/RIU, or 0.4 nm/% of water), good detection limit (i.e., 5×10^{-3} RIU, or ~10% of water), excellent resolution (i.e. 6×10^{-4} RIU, or 1.6% of water), and good reliability (%CV<1%) to be achieved in a sub-nanoliter probed volume of 168 fL.

Results and discussion

Design and fabrication of 1D-PhCs with high-order photonic bandgaps

Figure 1a shows a sketch of the ultra-high-order 1D-PhCs described in this work, which consist of periodic, vertical crystalline-silicon walls separated by air-gaps. The 1D-PhCs were designed according to the hybrid quarter-wave stack,[44] with thickness d_{Si} of the silicon walls and width d_{Air} of the air-gaps satisfying the phase matching conditions $d_{Si} = H\lambda_0/4n_{Si}$ and $d_{Air} = L\lambda_0/4n_{Air}$, where H and L (odd integer numbers) are independent design parameters, n_{Si} is the silicon refractive index at the operation wavelength λ_0 (air refractive index is 1), and m = (H+L)/2 is the order of the PBG that is centered at λ_0. Specifically, we designed 1D-PhCs with a pitch of either 10 or 20 μm featuring the 19th and 34th order PBGs centered at λ_0 = 1.65 μm and 1.6 μm, respectively, where silicon has a refractive index of ~3.45 RIU and negligible optical absorption. Design parameters were H=19 and L=19, which correspond to 2.3-μm-thick silicon walls and 7.7-μm-wide air-gaps, for PhCs with pitch of 10 μm; H=25 and L=43, which correspond to 2.8-μm-thick silicon walls and 17.2-μm-wide air-gaps, for those with pitch of 20 μm. Once these parameters are chosen, the morphology of the PhC structure is uniquely determined by its periodicity $D = d_{Si} + d_{Air}$ (10 and 20 μm), porosity $P = d_{Air}/D$ (0.77 and 0.86), and depth h=50 μm for both the PhCs to facilitate coupling with readout optical fibers.

Figure 1b shows a sketch of the main technological steps required for the fabrication of high-order silicon/air 1D-PhCs by using ECM. The initial material is an n-type silicon substrate of orientation (100), with a 100-nm-thick silicon dioxide (SiO_2) layer on top. The pattern of the microstructures to be fabricated is defined on a photoresist layer by UV-lithography, transferred to the SiO_2 by buffered hydrofluoridric acid (BHF) etching through the photoresist mask (Fig. 1b-2), replicated into the silicon surface by potassium hydroxide (KOH) etching through the SiO_2 mask (Fig. 1b-3), and then deeply etched into the silicon substrate by electrochemical etching (ECE) (Fig. 1b-4,5) [43]. Specifically, the ECE consists of a single etching step with an initial anisotropic phase (Fig. 1b-4), used to etch the pattern deep into the substrate and create high aspect-ratio microstructures, and a final isotropic phase (Fig. 1b-

5), used to release some of the etched microstructures from the substrate and, eventually, remove them. In fact, both functional and sacrificial structures were exploited to ensure high accuracy in fabrication of 1D-PhCs with a pitch of 10 and 20 μm. More in detail, functional structures are, by definition, parts of the microstructures that are anchored (partially, at least) to the Si-substrate after the isotropic phase of the electrochemical etching step; sacrificial structures are, by definition, parts that are not anchored to the Si-substrate after the isotropic phase of the electrochemical etching step and are, hence, removed. More than 20 replicas of high-order 1D-PhCs separated by a suitable anchor structure were successfully integrated on the same silicon substrate (size 0.5 cm x 1cm) (Figure S1). Figure 1c-f show scanning electron microscopy (SEM) images of two representative high-order 1D-PhCs with pitch 10 and 20 μm and porosity 0.77 and 0.85, respectively. From these images, the high quality of the microfabrication, in terms of both etching uniformity/accuracy and surface roughness, can be appreciated.

Optical characterization of 1D-PhCs with high-order bandgaps

A thorough optical characterization of high-order 1D-PhCs was carried out by measuring the reflected optical power spectrum in the range 1.0-1.7 μm at orthogonal incidence, using the fiber-optic setup reported in Figure S2, both in air and with a liquid, namely water and ethanol, filling the PhC air-gaps. Notice that, the high refractive index contrast between silicon and liquid to be analyzed limits light propagation through the 1D-PhC structure to a few periods.[39] Considering a worst-case scenario in which 20 silicon-wall/air-gap periods of the PhC contribute to form the reflectivity spectrum through light-matter interaction, the effective volume of liquid infiltrating the 20 periods of a PhC with pitch of 20 μm is smaller than 6.8 nL, whereas the probed volume (i.e. the volume of liquid actually probed by the optical fiber) is less than 168 fL. For each different medium, 9 power spectra were acquired so as to infer on measurement reproducibility (Figure S3). Experimental reflectivity spectra are then obtained by normalization of reflected optical power spectra with respect to a reference mirror.[24] Typical experimental reflectivity spectra of as-fabricated high-order 1D-PhCs with D=10 μm and D=20 μm are

shown in Figure 2a, superposed to theoretical reflectivity spectra calculated using the Transfer Matrix Method (TMM). This latter was modified (see Supplementary Information for details) to take into account the effects of both finite resolution bandwidth (RB) of the optical spectrum analyser [44] and scattering losses induced by the presence of rough silicon/air interfaces.[45]

Figure 2a shows an excellent agreement between theoretical spectra and experimental spectra measured on a PhCs with pitch of 10 and 20 μm, in terms of both reflectivity and spectral position of PBGs and notches. Remarkably, the reflectivity value within the PBGs, especially at wavelengths higher than 1.2 μm, is close to the ideal value of 0 dB (e.g. 0.63 dB for the PBG centered at λ=1.6 μm), suggesting that optical losses due to cumulative scattering over multiple silicon/air interfaces is negligible. Best-fitting of the 1D-PhC experimental reflectivity spectra acquired in air with theoretical reflectivity spectra over the full spectral range 1.0-1.7 μm yielded porosity values P=0.7718 and P=0.8563 for 1D-PhCs with pitch of 10 and 20 μm, respectively, which are in good agreement to design parameters, RB=9 nm, which well agrees with the resolution bandwidth of the optical spectrum analyser, and a surface roughness of 5 nm (root mean square value), which is significantly smaller than that of other micromachining technologies (e.g. reactive ion etching).[46]

To gain a deeper insight into the optical quality of the ECM-fabricated high-order 1D-PhCs, we performed higher resolution reflectivity measurements around λ=1.31 μm and λ=1.53 μm, where the PhC with pitch of 20 μm exhibits two deep reflectivity notches, as shown in Figure S4 and Figure 2b, respectively. A high quality-factor Q, namely 3830 (λ = 1.5326 μm, FWHM~0.4 nm) and 6300 (λ=1.308 μm, FWHM~0.2 nm), is experimentally measured for both the reflectivity notches, which is higher than that of PhCs exploiting low-order PBGs and comparable to that achieved with PhC resonant cavities. This result further demonstrates the excellent optical quality of ECM-fabricated high-order 1D-PhCs.

Figure 2c shows reflectivity spectra, both experimental and theoretical ones, of the 1D-PhCs with pitch of 20 μm upon infiltration with water (top) and ethanol (bottom). The line shape of the reflectivity spectrum of PhCs infiltrated with liquids is significantly different from that of PhCs in air. This is due to

the large increase of the refractive index from air to water and ethanol, which raises the order of the photonic bandgaps appearing in the wavelength range under investigation. Conversely, the refractive index variation between water and ethanol is not large enough to modify the line shape of the PhC reflectivity spectrum, though a clear red-shift of both reflectivity peaks and notches is apparent when water is replaced with ethanol.

Notice that, infiltration of 1D-PhCs with filling media of well-known optical properties, e.g. ethanol and water for which refractive index and absorption coefficient have been thoroughly investigated,[47] allows to further validate the morphological features of ECM-fabricated 1D-PhCs, through a comparison of experimental reflectivity spectra acquired upon infiltration of the model liquids with theoretical reflectivity spectra calculated (taking into account the model liquids) using for porosity, roughness, and resolution bandwidth the same values achieved for as-fabricated 1D-PhCs in air. Indeed, in Figure 2c an excellent agreement between experimental and theoretical spectra is apparent, these latter being calculated using porosity, surface roughness, and resolution bandwidth values above achieved by best-fitting of the reflectivity spectrum of empty PhCs in Figure 2a, namely 0.8563 for porosity, 5 nm for surface roughness, and 9 nm as resolution bandwidth.

In order to quantify the degree of tuning (DoT) of ECM-fabricated 1D-PhCs we defined as figure of merit $DoT\% = 100 \times \left[1 - \left(\lambda_{theo} - \lambda_{exp}\right)/\lambda_{theo}\right]$, where, λ_{theo} and λ_{exp} indicates the spectral position of either a peak (i.e. the central position of a PBG) or a notch in both theoretical and experimental reflectivity spectra. Figure 2d summarizes the DoT values achieved for high-order 1D-PhCs with pitch of 20 μm upon infiltration with water (blue bars) and ethanol (green bars). Remarkably, the DoT values are 99.8±0.1 % and 99.7 ±0.1 % for water and ethanol, respectively, which are very close to the ideal value of 100%. These results further demonstrate the excellent quality of high-order 1D-PhCs fabricated by ECM technology.

Chemical analysis using high-order 1D-PhCs as refractometric transducers

High-order PhCs with pitch of 20 μm were eventually investigated as refractometric transducers for chemical analysis of water-ethanol mixtures by leveraging the high sensitivity of high order reflectivity notches to tiny refractive index variation of a liquid filling the PhC air-gaps. Water-ethanol mixtures at different water concentrations from 0 to 100% were used to infiltrate the PhC and vary, in turn, the refractive index of the liquid filling the PhC air-gaps with high accuracy. A calibrated volume (400 nL) of the mixture was dropped on top of the silicon die to fill all the 20 replicas of high-order 1D-PhCs, then the reflectivity of a single 1D-PhC with ~100 periods was measured in the spectral range 1.1-1.7 μm (spectral resolution $\Delta\lambda$=0. 3 nm), where the PhC with pitch of 20 μm exhibits several reflectivity notches. It is convenient to remind here that, the volume of liquid infiltrating a single PhC of the array is much smaller, with a detection volume of about 168 fL being probed through the fiber-optic setup. For any water concentration three measurements were performed on three drops, at least, so as to take potential drop-to-drop variability into account. Variations of the notch positions due to both residuals left within the PhC upon evaporation of infiltrated mixtures and misalignments between readout fiber and PhC structure are ruled out by comparison of the reflectivity spectra acquired (in air) after evaporation of each drop of the mixture, with the reference reflectivity spectrum acquired on as-fabricated PhC (i.e. in air, before infiltration of any liquid). A representative series of reflectivity spectra is reported in Figure 3a for the experiment with water. Remarkably, the reflectivity spectrum measured after water evaporation is well superimposed to the reference spectrum before water infiltration over the entire spectral range 1.1-1.7 μm. A statistical analysis on the distribution of wavelength positions of several (namely, 18) reflectivity notches in the wavelength range 1.1-1.7 μm, carried out on reflectivity spectra acquired in air both after 23 infiltration/evaporation cycles and before starting infiltration (i.e. on as-fabricated PhCs), shows an absolute variation in the wavelength position of the notches (with respect to reference positions) that averages ~1 nm (average relative variation ~0.07%) (Figure S5). This neatly demonstrates that effects of both evaporation of infiltrated mixtures from the PhC air-gaps and possible misalignments of the relative position between optical fiber and PhC are negligible.

Figure 3b shows experimental calibration curves of high-order 1D-PhCs as refractometric transducers, namely spectral position (mean value and standard deviation) of 20 different reflectivity notches versus the water content in the water-ethanol mixture filling the PhC air-gaps. The wavelength notch positions were calculated by application of a numerical moving-average filter to the experimental data, so as to increase the signal-to-noise ratio and reduce, in turn, the effect of thermal noise on the notch position. Remarkably, the spectral position of all the reflectivity notches in the wavelength range 1.1-1.7 μm shift towards shorter wavelengths as the water concentration increases from 0 to 100%, in agreement with the reduction of the water-ethanol refractive index. This latter was calculated using the Lorentz–Lorentz law, also taking the spectral dispersion of the refractive index of both water and ethanol into account (Figure S6).[47,48] As shown in Figure 3b and Figure S7a, high-order 1D-PhCs have a sigmoidal response as a function of water content in ethanol, which is due to volume contraction of the water–ethanol mixture at water concentration of 10-30%, thus resulting in a nonlinear correlation between the refractive index of the mixture and concentration of water.[12,48]

Refractometric analytical performance of high-order 1D-PhCs for water quantification in water-ethanol mixtures are given in terms of reproducibility, sensitivity, resolution, and limit of detection, for each reflectivity notch in the wavelength range 1.1-1.7 μm. Reproducibility is evaluated using the coefficient of variation $\%CV = \sigma/\mu \times 100$, with σ standard deviation and μ mean value of the notch spectral positions; sensitivity S is calculated as the slope of the linear curve best-fitting the experimental calibration curve in the range 20-90% of water in ethanol; resolution R is calculated as $R = 3\,\sigma_{avg}/S$, being σ_{avg} average standard deviation of the notch positions experimentally measured for water fraction from 20 to 90%; limit od detection (LoD) is calculated as the value of either water concentration or water-ethanol refractive index for which the sigmoidal function best-fitting the experimental calibration curve intercepts the noise (N) level of the system $N = 3\sigma_{EtOH}$, with σ_{EtOH} being the standard deviation of the notch position experimentally measured in ethanol.

All the reflectivity notches taken into account in Figure 3b feature an excellent reliability (%CV<1%), with sensitivity S from 625±58 nm/RIU (0.2±0.02 nm/% of water) to 1140±145 nm/RIU (0.45±0.06 nm/% of water) (Figure 3c), which is comparable to best state-of-the-art integrated refractive index sensors; resolution R from $2.5\times10^{-3}\pm3\times10^{-4}$ RIU (6.8±0.6% of water) to $5.0\times10^{-3}\pm7\times10^{-4}$ RIU (12±2% of water) (Figure 3d) and limit of detection LoD from 0.014 RIU (40% of water in ethanol) to 0.02 RIU (50% of water in ethanol) (Figure S7b).

Notice that, the high LoD value can be explained in terms of quantization error due to a finite spectral resolution of the optical spectrum analyzer, amplitude stability (2 mdB/min) of the wideband light source used for large spectrum acquisition, and thermal noise due to room-temperature measurements on 1D-PhC structures without temperature control loop. In fact, given the poor sensitivity value of the sigmoidal curve for small water concentrations, the high standard deviation value σ_{EtOH} of the reference liquid (i.e. ethanol) due to the above reported reasons, leads to an unavoidably high LoD value.

To better infer into the LoD value achievable with high-order 1D-PhCs for water quantification in water-ethanol mixtures, we carried out refractometric measurements at higher spectral resolution (i.e., $\Delta\lambda$=0.05 nm) and improved light source stability (0.08 mdB/min). Specifically, we focused our attention to the reflectivity notch at λ~1.54 μm, in water, of a high-order 1D-PhC with pitch of 20 μm. Figure 3e shows a representative sequence of experimental reflectivity spectra collected upon infiltration of the air-gaps with water-ethanol mixtures at different water concentrations. Notice that, due to the reduced refractive index contrast of the PhC structure upon infiltration with liquid, the quality factor Q of the reflectivity notch reduces with respect to the value measured on 1D-PhC in air (i.e. as-prepared). Nonetheless, a blue-shift of the notch position is clearly evident as the concentration of water in the mixture increases from 0% (ethanol) to 100% (water), which well agrees with the decreased effective refractive index of the mixture as the water concentration increases.

Figure 3f reports the calibration curve, i.e. notch position versus water concentration/refractive index of the mixture, experimentally achieved over three different measurements on the same device of Figure 3e. Higher resolution spectral measurements confirm that the high-order 1D-PhC has a sigmoidal calibration curve with a clear initial plateau at water concentration below 10%, in agreement with the literature.[12,43] Accordingly, the limit of detection calculated at N= $3\sigma_{EtOH}$ is estimated to be 5×10^{-3} RIU (~13% of water in ethanol). At water concentration between 10 and 90%, the PhC transducer has a good linear response with both sensitivity S as high as 1000±32 nm/RIU (~0.40±0.01 nm/%) and resolution R as low as $6 \times 10^{-4} \pm 1 \times 10^{-4}$ RIU (1.6±0.2 % of water in ethanol), thus demonstrating that high-order PhCs can be successfully for reliable detection of water in water-ethanol mixture by refractometry, thus foreseeing possible industrial applications in pharmaceutics, biology, chemistry, biofuel, and food.

Conclusions

In this work we showed that ECM-fabricated high-order bandgaps 1D-PhCs as refractometric transducers enable high-sensitivity and high-reliability chemical analysis of water-ethanol mixtures.

ECM technology allows the fabrication of high-quality vertical silicon/air 1D-PhCs with ultra-high-order (up to 50th) photonic bandgaps in the near-infrared region to be accomplished. As a matter of fact, experimental reflectivity spectra acquired on ECM-fabricated high-order 1D-PhCs both as-prepared and infiltrated with model liquids, are in excellent agreement with theoretical spectra calculated using the TMM, modified to take light scattering due to rough silicon/air interfaces into account. Moreover, the small surface roughness of ECM-fabricated high-order 1D-PhCs (about 5 nm) enables high reflectivity bandgaps (~0.6 dB) separated by deep notches with high Q-factor (up to 6300) to be achieved. Finally, trace of water in ethanol with a detection limit of about 10% and resolution of about 1.5% can be reliably monitored over the range 10-100% in a sub-nanoliter detection volume of 168 fL.

Materials and methods

Substrates and chemicals. The fabrication of high-order 1D-PhCs was carried out on 725-µm-thick *n*-doped silicon substrates (crystalline orientation <100>, resistivity 3–8 Ω·cm) with 200-nm-thick SiO_2 on top (STMicroelectronics). All the chemicals (Sigma Aldrich) were reagent grade.

Seed-pattern generation. UV-lithography was used to define the seed-pattern on the SiO_2 layer. Specifically, a 1.8-µm-thick film of positive photoresist (Shipley, S1818) was spin-coated at 5000 rpm for 60 s on the substrate. After a soft-baking step (115 °C, 90 s), a contact-lithography system (Karl–Suss, MJB3) was used to shine UV-light against the photoresist through a chromium mask. The exposed photoresist was removed by rinsing the sample into a developer solution and a post-baking procedure (115°C, 90 s) was performed to increase the stability of the pattern. The seed-pattern was transferred to the SiO_2 layer by wet etching in BHF solution for 120 s. Finally, a wet etching step in a 25% KOH solution, saturated with isopropanol to enhance the etching uniformity, was performed at 50°C for 30 minutes to transfer the pattern into the Si-substrate trough the SiO_2 mask. Once the generation of the seed-pattern was complete, the SiO_2 layer was removed with a 1:1 HF (48%):ethanol solution.

Electrochemical etching (ECE). The experimental setup used for the electrochemical etching of silicon is detailed in our previous work.[43] The volumetric composition of the electrolyte used during ECE was 5% HF and 95% H_2O. To enhance the etching uniformity 1000 ppm of Sodium Lauryl Sulfate, which reduces the formation of hydrogen bubbles at the etched surface, was added to the electrolyte and the solution was stirred during ECE. The entire etching process was performed at a constant voltage of 1.2V, whereas the etching current was adjusted over-time to control the morphology of the etched structures. During the anisotropic phase, the etching current was linearly reduced from 23.21 to 19.71 mA in order to obtain perfect vertical Si microstructures. The etching time of the anisotropic phase (2100 s) was chosen to fully etch 50–µm-deep vertical structures. To switch into the isotropic regime, the etching current was suddenly increased from 19.71 to 32.71 mA and kept constant for the next 200 s. The etching time of the isotropic phase was long enough to completely release the sacrificial structures.

Morphological characterization. Morphology and shape of the high-order 1D-PhCs were investigated by scanning electron microscopy. To this end, images with prospective views of the long-period vertical silicon/air 1D-PhCs were acquired using a scanning electron microscope (JEOL, JSM-6390) at an acceleration voltage of 3kV.

Optical characterization and refractometry application. A scheme of the experimental setup for spectral reflectivity measurements is shown in Figure S2. A bidirectional 2x2 single mode fiber-coupler (coupling ratio 50:50) was used to carry broadband radiation toward the PhC and to redirect the back-reflected light toward the monochromator of an optical spectrum analyser, i.e. OSA Agilent 86142B and ANDO AQ6317 for measurements with resolution bandwidth of 10 nm and 10 pm, respectively. A pigtail style focuser with an aspheric lens (OzOptics, spot-diameter 50 μm and working distance 23.5 mm) was used as readout termination. An APC/FC connector was connected to the unused output of the coupler to avoid spurious back-reflections. The PhC was mounted on a XYZ stage and the readout lens was secured on a kinematic mount. Alignment of the pigtail focuser with the PhC is achieved by maximizing the optical power reflected back by the PhC and collected at the optical spectrum analyser, which ensures both spatial (XYZ) and angular (TETA) alignments.

A Tungsten lamp was used as white light source in the wavelength range 1.0 -1.7 μm, whereas a diode-pumped Er3+-doped fiber with a flat-top spectrum centered at 1.548 μm was used for finer reflectivity measurement. To reduce the level of random noise, each collected reflectivity spectrum was obtained by averaging 10 different measures.

Acknowledgments

This research did not receive any specific grant from funding agencies in the public, commercial, or not-for-profit sectors.

Supporting Information.

Supporting Information Available: The following files are available free of charge.

SupplementaryInformation.pdf. SEM images of high-order 1D-PhCs, schematic of the fiber-optic setup, theoretical spectral reflectivity of 1D-PhC with rough interfaces; reflectivity measurements, assessment of the protocol for refractometry with the high-order 1D-PhCs, calculated refractive indices of water-ethanol mixtures; further PhC refractometry with wideband light source.

References

(1) Onuki, S.; Koziel, J. A.; Jenks, W. S.; Cai, L.; Grewell, D.; Leeuwen, J. H. Van. Taking Ethanol Quality beyond Fuel Grade : A Review. **2016**, *122*, 588–598.

(2) Jung, H. S.; Verwilst, P.; Kim, W. Y.; Kim, J. S. Fluorescent and Colorimetric Sensors for the Detection of Humidity or Water Content. *Chem. Soc. Rev.* **2016**, *45* (5), 1242–1256.

(3) Mitchell, J.; Smith, D. M. *Aquametry: A Treatise on Methods for the Determination of Water*, 2nd ed.; Wiley: New York, 1977.

(4) Plutowska, B.; Wardencki, W. Application of Gas Chromatography-Olfactometry (GC-O) in Analysis and Quality Assessment of Alcoholic Beverages - A Review. *Food Chem.* **2008**, *107* (1), 449–463.

(5) Mendes, L. S.; Oliveira, F. C. C.; Paulo A.Z. Suarez; Rubim, J. C. Determination of Ethanol in Fuel Ethanol and Beverages by Fourier Transform (FT)-near Infrared and FT-Raman Spectrometries. *Anal. Chim. Acta* **2003**, *493* (2), 219–231.

(6) Ohira, S. I.; Goto, K.; Toda, K.; Dasgupta, P. K. A Capacitance Sensor for Water: Trace Moisture Measurement in Gases and Organic Solvents. *Anal. Chem.* **2012**, *84* (20), 8891–8897.

(7) Vello, T. P.; De Oliveira, R. F.; Silva, G. O.; De Camargo, D. H. S.; Bufon, C. C. B. A Simple Capacitive Method to Evaluate Ethanol Fuel Samples. *Sci. Rep.* **2017**, *7*, 1–7.

(8) Kim, B. C.; Yamamoto, T.; Kim, Y. H. In-Line Measurement of Water Content in Ethanol Using a PVA-Coated Quartz Crystal Microbalance. *Sensors* **2014**, *14* (1), 1564–1575.

(9) Koirala, G. R.; Dhakal, R.; Kim, E. S.; Yao, Z.; Kim, N. Y. Radio Frequency Detection and Characterization of Water-Ethanol Solution through Spiral-Coupled Passive Micro-Resonator Sensor. *Sensors* **2018**, *18* (4), 1–10.

(10) Qin, P. Z.; Han, C. H.; Huang, D. W. A Fluorescent Probe for Water Content in Ethanol Based on a Complex of Ruthenium(Ii). *Anal. Methods* **2014**, *6* (1), 202–206.

(11) Dong, Y.; Cai, J.; Fang, Q.; You, X.; Chi, Y. Dual-Emission of Lanthanide Metal-Organic

Frameworks Encapsulating Carbon-Based Dots for Ratiometric Detection of Water in Organic Solvents. *Anal. Chem.* **2016**, *88* (3), 1748–1752.

(12) Fujiwara, E.; Takeishi, R. T.; Hase, A.; Ono, E.; Santos, J. S.; Suzuki, C. K. Real-Time Optical Fibre Sensor for Hydro-Alcoholic Solutions. *Meas. Sci. Technol.* **2010**, *21* (9), 094035. DOI: 10.1088/0957-0233/21/9/094035.

(13) Wijaya, Y. N.; Kim, J.; Hur, S. H.; Park, S. H.; Kim, M. H. Metal Nanocrystal-Based Sensing Platform for the Quantification of Water in Water-Ethanol Mixtures. *Sensors Actuators, B Chem.* **2018**, *263*, 59–68.

(14) Guo, Y.; Li, H.; Reddy, K.; Shelar, H. S.; Nittoor, V. R.; Fan, X. Optofluidic Fabry-Ṕrot Cavity Biosensor with Integrated Flow-through Micro-/Nanochannels. *Appl. Phys. Lett.* **2011**, *98* (4), 3–5.

(15) Surdo, S.; Carpignano, F.; Strambini, L. M.; Merlo, S.; Barillaro, G. Capillarity-Driven (Self-Powered) One-Dimensional Photonic Crystals for Refractometry and (Bio) Sensing Applications. *RSC Adv.* **2014**, *4*, 51935–51941.

(16) Fenzl, C.; Hirsch, T.; Wolfbeis, O. S. Photonic Crystal Based Sensor for Organic Solvents and for Solvent-Water Mixtures. *Sensors (Switzerland)* **2012**, *12*, 16954–16963.

(17) Arif, M. F. H.; Biddut, M. J. H.; Babu, M. S. I.; Rahman, H. M. M.; Rahman, M. M.; Jahan, B.; Chaity, M. S.; Khaled, S. M. Photonic Crystal Fiber Based Sensor for Detecting Binary Liquid Mixture. *Opt. Photonics J.* **2017**, *7* (11), 221–234.

(18) Surdo, S.; Merlo, S.; Carpignano, F.; Strambini, L. M.; Trono, C.; Giannetti, A.; Baldini, F.; Barillaro, G. Optofluidic Microsystems with Integrated Vertical One-Dimensional Photonic Crystals for Chemical Analysis. *Lab Chip* **2012**, *12* (21), 4403–4415.

(19) Threm, D.; Nazirizadeh, Y.; Gerken, M. Photonic Crystal Biosensors towards On-Chip Integration. *J. Biophotonics* **2012**, *16*, 1–16.

(20) Zhao, Y.; Zhao, X.; Gu, Z. Photonic Crystals in Bioassays. *Adv. Funct. Mater.* **2010**, *20*, 2970–

2988.

(21) Inan, H.; Poyraz, M.; Inci, F.; Lifson, M. A.; Baday, M.; Cunningham, B. T.; Demirci, U. Photonic Crystals: Emerging Biosensors and Their Promise for Point-of-Care Applications. *Chem. Soc. Rev.* **2017**, *46*, 366–388.

(22) De Stefano, L.; Moretti, L.; Rendina, I.; Rossi, A. M. Porous Silicon Microcavities for Optical Hydrocarbons Detection. *Sensors Actuators, A Phys.* **2003**, *104* (2), 179–182.

(23) Mulloni, V.; Pavesi, L. Porous Silicon Microcavities as Optical and Electrical Chemical Sensors. *Appl. Phys. Lett.* **2000**, *76* (18), 2535–2525.

(24) Zhang, Y. N.; Zhao, Y.; Zhou, T.; Wu, Q. Applications and Developments of On-Chip Biochemical Sensors Based on Optofluidic Photonic Crystal Cavities. *Lab Chip* **2017**, *18* (1), 57–74.

(25) Baker, J. E.; Sriram, R.; Miller, B. L. Two-Dimensional Photonic Crystals for Sensitive Microscale Chemical and Biochemical Sensing. *Lab Chip* **2015**, 971–990.

(26) Skivesen, N.; Têtu, A.; Kristensen, M.; Kjems, J.; Frandsen, L. H.; Borel, P. I. Photonic-Crystal Waveguide Biosensor. *Opt. Express* **2007**, *15* (6), 3169–3176.

(27) Amsden, J. J.; Perry, H.; Boriskina, S. V.; Gopinath, A.; Kaplan, D. L.; Dal Negro, L.; Omenetto, F. G. Spectral Analysis of Induced Color Change on Periodically Nanopatterned Silk Films. *Opt. Express* **2009**, *17* (23), 21271–21279.

(28) Huang, M.; Yanik, A. A.; Chang, T.-Y.; Altug, H. Sub-Wavelength Nanofluidics in Photonic Crystal Sensors. *Opt. Express* **2009**, *17* (26), 24224–24233.

(29) De Stefano, L.; Rendina, I.; Moretti, L.; Tundo, S.; Rossi, A. M. Smart Optical Sensors for Chemical Substances Based on Porous Silicon Technology. *Appl. Opt.* **2004**, *43* (1), 167–172.

(30) Mortensen, N. A.; Xiao, S.; Pedersen, J. Liquid-Infiltrated Photonic Crystals: Enhanced Light-Matter Interactions for Lab-on-a-Chip Applications. *Microfluid. Nanofluidics* **2008**, *4*, 117–127.

(31) Fan, X.; White, I. M. Optofluidic Microsystems for Chemical and Biological Analysis. *Nat.*

Photonics **2011**, *5* (10), 591–597.

(32) Grimaldi, I. A.; Testa, G.; Bernini, R. Flow through Ring Resonator Sensing Platform. *RSC Adv.* **2015**, *5* (86), 70156–70162.

(33) Xu, T.; Zhu, N.; Xu, M. Y.-C.; Wosinski, L.; Aitchison, J. S.; Ruda, H. E. Pillar-Array Based Optical Sensor. *Opt. Express* **2010**, *18* (6), 5420–5425.

(34) Lee, M. R.; Fauchet, P. M. Two-Dimensional Silicon Photonic Crystal Based Biosensing Platform for Protein Detection. *Opt. Express* **2007**, *15* (8), 4530–4535.

(35) St-Gelais, R.; Masson, J.; Peter, Y.-A. All-Silicon Integrated Fabry–Pérot Cavity for Volume Refractive Index Measurement in Microfluidic Systems. *Appl. Phys. Lett.* **2009**, *94* (24), 243905. DOI: 10.1063/1.3152286.

(36) Luchansky, M. S.; Bailey, R. C. High- Q Optical Sensors for Chemical and Biological Analysis. *Anal. Chem.* **2012**, *84* (2), 793–821.

(37) Hagino, H.; Takahashi, Y.; Tanaka, Y.; Asano, T.; Noda, S. Effects of Fluctuation in Air Hole Radii and Positions on Optical Characteristics in Photonic Crystal Heterostructure Nanocavities. *Phys. Rev. B* **2009**, *79*, 1–8.

(38) Peng, W.; Chen, Y.; Ai, W. Higher-Order Mode Photonic Crystal Based Nanofluidic Sensor. *Opt. Commun.* **2017**, *382*, 105–112.

(39) Surdo, S.; Carpignano, F.; Silva, G.; Merlo, S.; Barillaro, G. An All-Silicon Optical Platform Based on Linear Array of Vertical High-Aspect-Ratio Silicon / Air Photonic Crystals. *Appl. Phys. Lett.* **2013**, *103*, 171103. DOI: 10.1063/1.3152286.

(40) Carpignano, F.; Surdo, S.; Barillaro, G.; Merlo, S. Silicon Micromachined Device Testing by Infrared Low-Coherence Reflectometry. *J. Microelectromech. Syst.* **2015**, *24* (6), 1960–1964.

(41) Polito, G.; Surdo, S.; Robbiano, V.; Tregnago, G.; Cacialli, F.; Barillaro, G. Two-Dimensional Array of Photoluminescent Light Sources by Selective Integration of Conjugated Luminescent Polymers into Three-Dimensional Silicon Microstructures. *Adv. Opt. Mater.* **2013**, *1* (12), 894–

898.

(42) Astrova, E. V; Fedulova, G. V. Formation of Deep Periodic Trenches in Photo-Electrochemical Etching of n-Type Silicon. *J. Micromech.Microeng.* **2009**, *19*, 095009. DOI: 10.1088/0960-1317/19/9/095009.

(43) Bassu, M.; Surdo, S.; Strambini, L. M.; Barillaro, G. Electrochemical Micromachining as an Enabling Technology for Advanced Silicon Microstructuring. *Adv. Funct. Mater.* **2012**, *22*, 1222–1228.

(44) Barillaro, G.; Strambini, L. M.; Annovazzi-lodi, V.; Merlo, S. Optical Characterization of High-Order 1-D Silicon Photonic Crystals. *IEEE J. Sel. Top. Quantum Electron.* **2009**, *15* (5), 1359–1367.

(45) Mitsas, C. L.; Siapkas, D. I. Of Coherent and Incoherent Reflectance and Surfaces , Interfaces , and Finite Substrates. *Appl. Opt.* **1995**, *34* (10), 1678–1683.

(46) Wu, B.; Kumar, A.; Pamarthy, S. High Aspect Ratio Silicon Etch : A Review. *J. Appl. Phys.* **2010**, *108*, 051101. DOI:10.1063/1.3474652.

(47) Kedenburg, S.; Vieweg, M.; Gissibl, T.; Giessen, H. Linear Refractive Index and Absorption Measurements of Nonlinear Optical Liquids in the Visible and Near-Infrared Spectral Region. **2012**, *25240* (2010), 6230–6240.

(48) Herráez, J. V.; Belda, R. Refractive Indices, Densities and Excess Molar Volumes of Monoalcohols + Water. *J. Solution Chem.* **2006**, *35* (9), 1315–1328.

Figures and captions

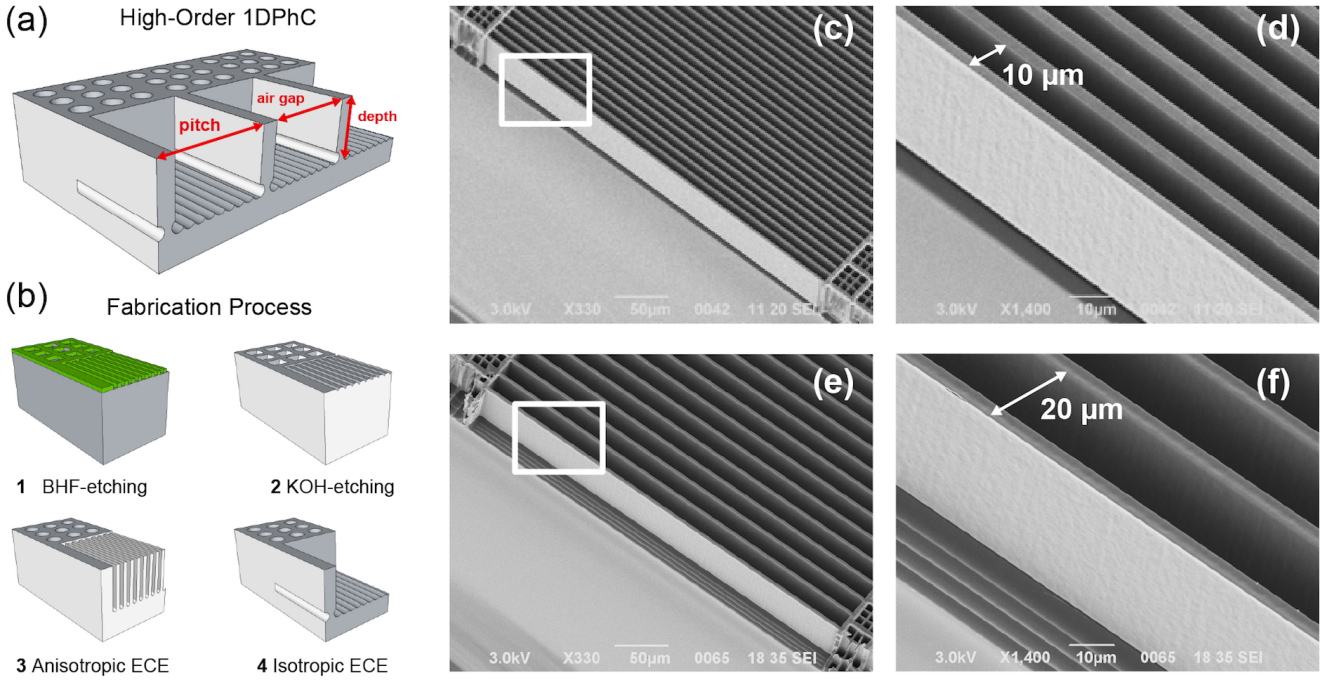

Figure 1. High-order 1D-PhCs concept and fabrication. (a) Schematic representation of the high-order 1D-PhC of this work (not to scale), consisting of periodic vertical silicon walls with depth of 50 µm separated by air-gaps with pitch up to 20 µm, that is 10 times larger than the operation wavelength. (b) Main technological steps for the fabrication of high-order 1D-PhC by ECM technology: 1- pattern definition on a silicon-dioxide layer on top of a Si substrate by standard lithography; 2- seed-pattern transfer on the Si surface by KOH-etching; 3- deep anisotropic etching of the pattern by electrochemical etching (ECE) and formation of functional microstructures; 4- isotropic etching of the etched pattern at the bottom and removal of sacrificial microstructures. (c-f) SEM bird-eye views (at different magnifications) of ECM-fabricated 1D-PhCs with height 50 µm and pitch 10 µm (c-d) and 20 µm (e-f). (d) and (f) show magnifications of (c) and (e), respectively, highlighting the excellent optical quality of the microfabricated structures.

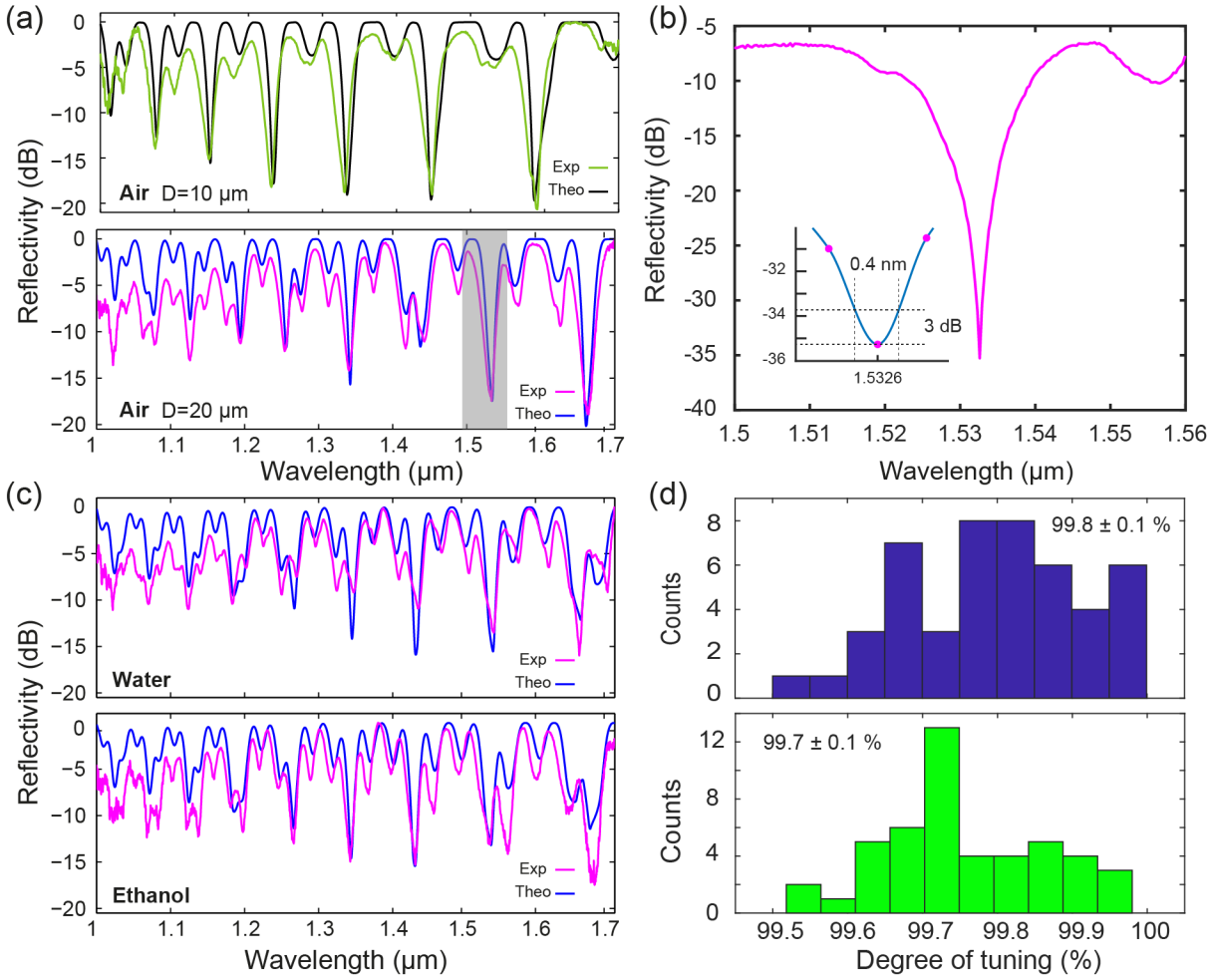

Figure 2. Optical characterization of high-order 1D-PhCs. (a) Experimental and theoretical reflectivity spectra of as-prepared high-order 1D-PhCs with pitch of 10 μm and 20 μm. (b) High-resolution acquisition of a deep (Q=3500) reflectivity notch of a 1D-PhC with pitch of 20 μm, centered at λ =1.5326 μm. (c) Comparison between experimental and theoretical spectra of high-order 1D-PhC with spatial period of 20 μm, upon infiltration with water and ethanol. (d) Distribution of the degree of tuning (DoT) of a high-order 1D-PhC with pitch of 20 μm infiltrated with water (blue bars) and ethanol (green bars).

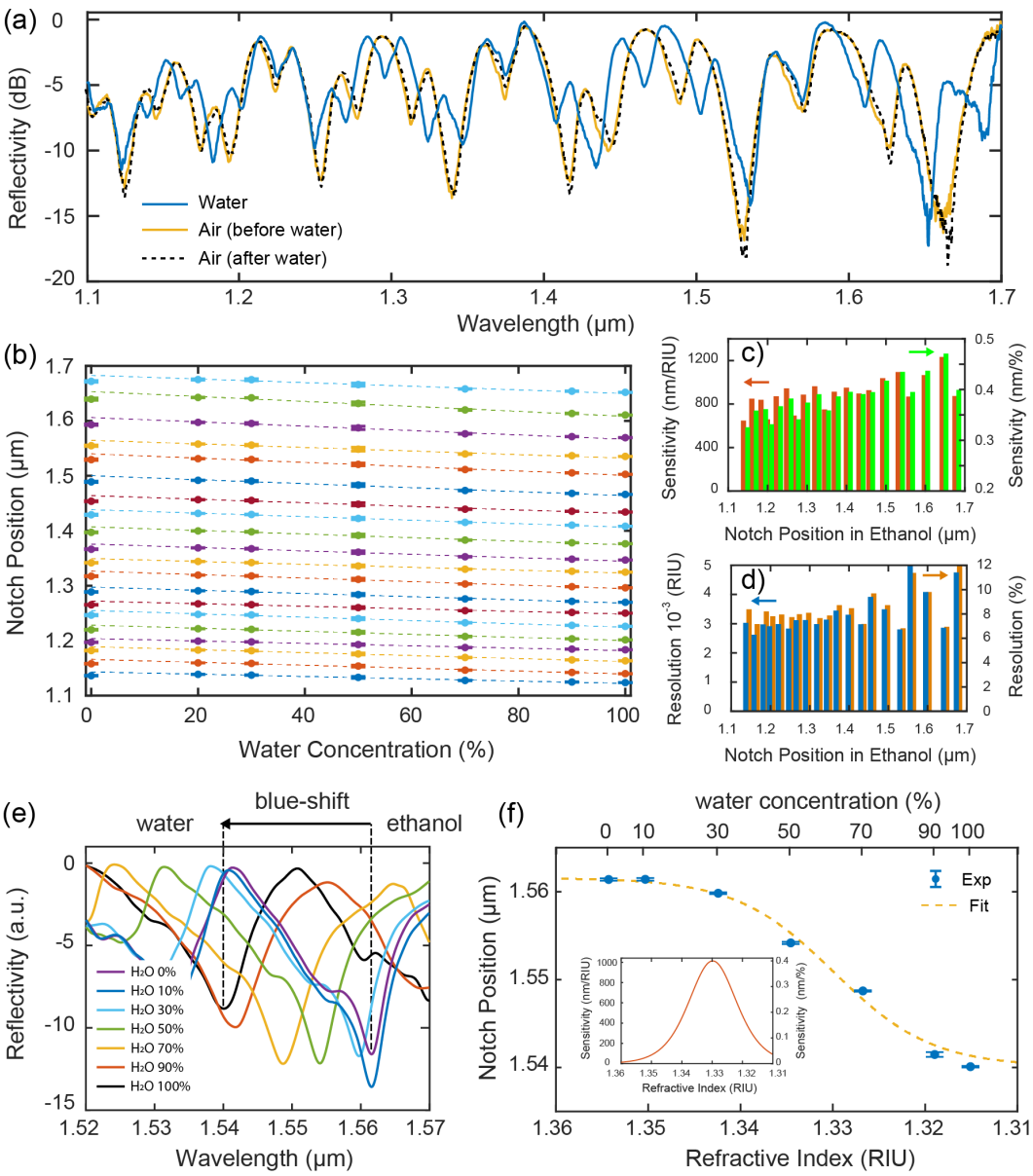

Figure 3. Chemical refractometric analysis with high-order 1D-PhCs. (a) Experimental reflectivity spectra of a high-order PhC with pitch of 20 μm: in air, before infiltration of the water-ethanol mixtures (solid yellow trace); with water infiltrating the air-gaps (solid blue trace); in air, after water evaporation (dashed black trace). (b) Notch wavelength positions (mean value and standard deviation) as a function of the water fraction of the mixture filling the PhC air-gaps. The dashed lines denote the linear curves best-fitting the experimental data in the range 20-90% of water content. Sensitivity (c) and resolution (d) associated with the reflectivity notches in the range 1.1-1.7 μm. (e) Sequence of normalized reflectivity spectra of a high-order 1D-PhC with pitch of 20 μm upon infiltration of ethanol-water mixtures at

different water concentrations. f) Wavelength notch position (mean value and standard deviation) as a function of both water concentration (top axis) and refractive index (bottom axis) of the mixture infiltrating the PhC. The dashed yellow trace represents the sigmoidal curve best-fitting the experimental data. The inset shows sensitivity vs. refractive index.

Table of Contents (TOC)

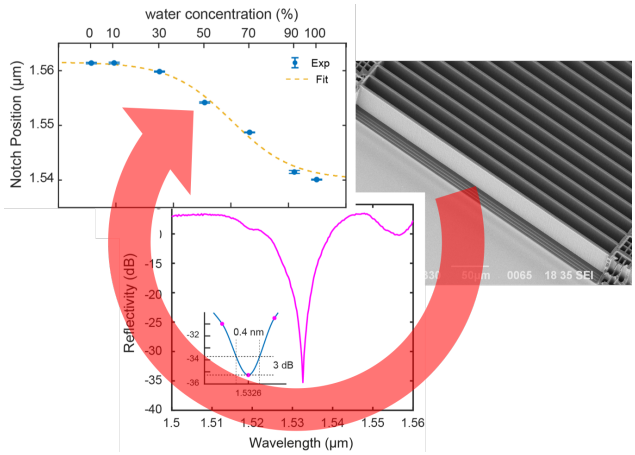

for TOC only